This article was downloaded by:
On: *25 January 2011*
Access details: *Access Details: Free Access*
Publisher *Taylor & Francis*
Informa Ltd Registered in England and Wales Registered Number: 1072954 Registered office: Mortimer House, 37-41 Mortimer Street, London W1T 3JH, UK

Liquid Crystals
Publication details, including instructions for authors and subscription information:
http://www.informaworld.com/smpp/title~content=t713926090

The geometrical optics approach for multidimensional liquid crystal cells

G. Panasyuk[a]; J. R. Kelly[b]; P. Bos[b]; E. C. Gartland Jr.[c]; D. W. Allender[d]
[a] Department of Bioengineering University of Pennsylvania Philadelphia PA 19104, USA, [b] Liquid Crystal Institute Kent State University Kent OH 44242, USA, [c] Department of Mathematical Sciences Kent State University Kent OH 44242, USA, [d] Department of Physics Kent State University Kent OH 44242, USA,

Online publication date: 11 November 2010

To cite this Article Panasyuk, G. , Kelly, J. R. , Bos, P. , Gartland Jr., E. C. and Allender, D. W.(2004) 'The geometrical optics approach for multidimensional liquid crystal cells', Liquid Crystals, 31: 11, 1503 — 1515
To link to this Article: DOI: 10.1080/02678290412331304078
URL: http://dx.doi.org/10.1080/02678290412331304078

PLEASE SCROLL DOWN FOR ARTICLE

Full terms and conditions of use: http://www.informaworld.com/terms-and-conditions-of-access.pdf

This article may be used for research, teaching and private study purposes. Any substantial or systematic reproduction, re-distribution, re-selling, loan or sub-licensing, systematic supply or distribution in any form to anyone is expressly forbidden.

The publisher does not give any warranty express or implied or make any representation that the contents will be complete or accurate or up to date. The accuracy of any instructions, formulae and drug doses should be independently verified with primary sources. The publisher shall not be liable for any loss, actions, claims, proceedings, demand or costs or damages whatsoever or howsoever caused arising directly or indirectly in connection with or arising out of the use of this material.

LIQUID CRYSTALS, VOL. 31, NO. 11, NOVEMBER 2004, 1503–1515

Taylor & Francis
Taylor & Francis Group

The geometrical optics approach for multidimensional liquid crystal cells

G. PANASYUK*, J. R. KELLY†, P. BOS†, E. C. GARTLAND, JR.‡ and D. W. ALLENDER§

Department of Bioengineering, University of Pennsylvania, Philadelphia, PA 19104, USA

†Liquid Crystal Institute, Kent State University, Kent, OH 44242, USA

‡Department of Mathematical Sciences, Kent State University, Kent, OH 44242, USA

§Department of Physics, Kent State University, Kent, OH 44242, USA

(*Received 7 May 2004; accepted 15 July 2004*)

We present an approach based on the geometrical optics approximation (GOA) for analysis of liquid crystal cells whose director varies in more than one spatial dimension (multidimensional liquid crystal cells). The GOA is applied to calculate light transmittance and far field diffraction patterns for two- and three-dimensional nematic liquid crystal films. Important features of the GOA, such as a method of eliminating non-convergence problems that can occur during the iterative numerical solution of the equations for the amplitudes of the electromagnetic field, are described. We compare the results obtained from the GOA with those produced by the quasi-one-dimensional Jones calculus and the beam propagation method, where the latter is applicable. It was found that the refraction (or ray bending) effects, produced by the GOA, are more important than effects of diffraction and light scattering, which means that the GOA (unlike the Jones calculus) is accurate for the considered type of liquid crystal cells, whose director varies on the micron scale. The GOA is about as fast as the Jones method and is applicable for calculating optical properties of liquid crystal cells with any number of dimensions of director variations.

Downloaded At: 16:42 25 January 2011

1. Introduction

The simplest approach for handling multidimensional optics involves extending one-dimensional techniques such as the 4×4 matrix methods [1] or the Jones calculus [2]. In these approaches, lateral variations in optical properties are ignored, and the multidimensional behaviour is then obtained as a composite of several one-dimensional calculations. This simple description is applicable when the wavelength of light λ is very small relative to the characteristic size of the director variations in transverse directions. At the other extreme, when this size is smaller or comparable to λ, rigorous methods must be employed. One of the most widely used is the so-called finite difference time domain (FDTD) method [3–5], which is a direct solution to the Maxwell curl equations. The time-harmonic form of the Maxwell equations can be solved directly as well, although different techniques are required [6]. Both of these methods suffer from a restriction on the size of problem that can be solved effectively; this is because a sufficient number of grid points per wavelength is required to model accurately the electromagnetic fields throughout the region. Another rigorous way of handling the multidimensional optics is the grating method (GM) [7, 8]. This approach can be applied to a LC cell periodic in the transverse (xy) plane, so that the dielectric tensor becomes a periodic function of x, y. Eventually, the GM gives a coupled system of first order ordinary differential equations for a set of the Fourier coefficients of the transverse electromagnetic field components, which can be considered as a vector $\mathbf{\Psi}$ in some space. This system describes the evolution of $\mathbf{\Psi}$ along the z-direction (normal to the cell substrates) and must be solved numerically. As is clear, when the number of Fourier harmonics that are taken into account by the method is large, one can produce a very accurate solution. At the same time, the matrix $\hat{A}$ that describes the evolution also becomes very large, and the calculation time could be prohibitively huge as in the case of use of the FDTD method for a cell with large linear sizes. Thus, it is desirable to have a fast and, at the same time,

*Author for correspondence; e-mail: georgey@seas.upenn.edu

Liquid Crystals ISSN 0267-8292 print/ISSN 1366-5855 online © 2004 Taylor & Francis Ltd
http://www.tandf.co.uk/journals
DOI: 10.1080/02678290412331304078

Downloaded At: 16:42 25 January 2011

reasonably accurate method to calculate the optical properties of multidimensional LC cells. One such method that has been recently proposed is the reduced grating method (RGM) [7, 8]. This innovative way of describing optics is based on the projection of the evolution matrix onto Krylov subspaces and the application of the singular-value decomposition. It is a modification of the GM, and can be shortly described as follows. The vector $\Psi(z=h)$ on the next z-level can be calculated as $\exp(\hat{A})\Psi(z=0)$ and requires the computation of a significant number of vectors $\mathbf{f}_k=\hat{A}^k\Psi(z=0)$, and is numerically inefficient. The main idea of the RGM is that vectors $\mathbf{f}_k$ are nearly linearly dependent, so a relatively small number of orthonormal vectors $\mathbf{u}_k$ are enough to span approximately the space produced by vectors $\mathbf{f}_k$. In such a situation, it is possible to obtain $\Psi(z=h)$ with a good accuracy and by 1–2 orders of magnitude faster (than the usual GM) using a projection matrix formed by this reduced set of $\mathbf{u}_k$ instead of the full $\hat{A}$ matrix. This was illustrated by application of the RGM to the light transmittance calculation for several 2D LC cells. However, no physical explanation as to why the RGM should work, except a good correspondence of its results to the GM ones, has been presented, and an additional study of properties of the RGM is desirable.

A wide angle beam propagation method (BPM) for two-dimensional liquid crystal optics problems [9–11] (including LC cells with a tilted–twisted director profile) is another interesting method, which is applicable when feature sizes are smaller or comparable to λ. The basic idea of the BPM is to replace the exact Maxwell equations for components of the electric or magnetic field by partial differential equations of parabolic type that admit an efficient numerical implementation. Although the equations so produced are not identical to the initial Maxwell equations, they retain the most important contributions from the Maxwell equations, and allow, in particular, one to describe with very good accuracy geometrical optics effects as well as processes of light scattering (or light diffusion). The technique is stable and fast in comparison with the FDTD approach. Unfortunately, this way of describing optics has the following important restriction: the plane of incidence of light must coincide with the plane of the director variations; this prevents the use of the method for studying optical properties of LC cells with a 3D director $\hat{n}$, as well as, for example, calculating the viewing angle diagram even in a 2D LC cell. The BPM, as well as the GOA and Jones calculus, also neglects reflections inside the LC structure. However, within the above-mentioned bounds, it was demonstrated [9–11] that the results of the BPM are in excellent agreement with the FDTD calculations even when the geometry is comparable in size to λ.

In this paper, another description of the multidimensional optics of liquid crystal media, based on the geometrical optics approximation (GOA), is presented. It is known [12] that the GOA is applicable if the ratio $\kappa=\lambda/2\pi l$ is small (here l is a characteristic scale of the medium inhomogeneity). As is shown here, the GOA, being about as fast as the Jones method, increases the range of the optical description to include the micron scale regime, where the latter approach loses its accuracy. Meyer and Ong [13, 14] were the first to apply the GOA to liquid crystals in one dimension. This approach was applied later to study ray trajectories and intensity variations for light propagating through a periodically distorted homogeneous nematic layer [15, 16]. The GOA has also been used to study ray trajectories in the equatorial plane of a nematic liquid crystal droplet with radial director configuration [17]. More recently, the GOA was successfully applied to study the electro-optical performance of a self-compensating vertically aligned liquid crystal display cell [18], and has been used to investigate optical properties of a switchable diffraction grating [19]. Finally, a mathematical formalism of the GOA applicable for a LC cell with a multidimensional director distribution $\hat{n}(\mathbf{r})$ has been considered, and an iterative solution for the GOA equations was found for a cell with a 3D director [20].

In this paper we describe shortly the mathematical apparatus of the GOA paying more attention to an important question related to removing from the model problems of non-convergence of iterative numerical solvers (§2). The presented formalism uses the 'field' approach, which is more convenient for computer coding than the 'ray' method, which is usually employed. Particular 2D and 3D cells were considered as examples of the GOA application (§3). A comparison between the results of calculations of the differential and averaged light transmittance, as well as the diffraction spectra produced by the GOA, BPM and Jones method, is also presented. We do not compare the GOA results directly with the results of the FDTD calculations, because, as was found earlier [9–11], there is an excellent correspondence between the BPM and FDTD, and in this study we assume that the BPM gives an accurate description (when it is applicable).

2. Mathematical formulation of the GOA

The GOA uses expansions for the electric and magnetic fields **E** and **H** in powers of $k_0{}^{-1}=\lambda/2\pi$:

$$\mathbf{E}(\mathbf{r})=\exp[\mathrm{i}k_0S(\mathbf{r})]\sum_{m=0}^{\infty}\mathrm{E_m}(r)/(\mathrm{i}k_0)^m \qquad (1)$$

with a similar expression for **H**. Here the function $S(\mathbf{r})$ is the optical path, or the eikonal. The surfaces of constant S are orthogonal to the local wave vector direction $\mathbf{n}(\mathbf{r}) \equiv \nabla S$ and are the wavefronts of geometrical optics. After substituting (1) into the time-harmonic wave equation for the electric field

$$\nabla^2 E_i - \nabla_i(\nabla E) = (\mathrm{i}k_0)^2 \varepsilon_{ik} E_k \tag{2}$$

where ε_{ik} is the dielectric tensor of the LC and summing over repeated indices is assumed throughout the paper; the lowest order terms give an eigenvalue equation for two eigenvectors **o** and **e**, which are the directions of polarization for the ordinary and extraordinary waves. Corresponding eigenvalues S_o and S_e (optical path lengths of the ordinary and extraordinary waves) satisfy equation $[(\nabla S_\mathrm{o})^2 - n_\mathrm{o}^2]\ [(\nabla S_\mathrm{e})^2 - (n_\mathrm{eff})^2] = 0$, where n_eff is the effective index of refraction (for details of the derivation see [20]). Thus, S_o satisfies $(\nabla S_\mathrm{o})^2 = n_\mathrm{o}^2$ and can be solved analytically, at least in cases with relatively simple cell geometries. The equation for S_e is

$$\partial_z S_\mathrm{e} = \left[\left(B^2 - AC\right)^{1/2} - B\right] \Big/ A \tag{3}$$

where the symbol ∂_z denotes differentiation with respect the z-coordinate (we assume that light propagates in some direction in the half space of increasing z), and the coefficients A, B, and C are determined by the following relations:

$$\begin{aligned} A &= 1 + \Delta\varepsilon(\hat{\boldsymbol{n}}_z)^2, \\ B &= \Delta\varepsilon\left(\hat{\boldsymbol{n}}_x \partial_x S_e + \hat{\boldsymbol{n}}_y \partial_y S_e\right), \\ C &= n_e^2 - (\partial_x S_e)^2 - \left(\partial_y S_e\right)^2 - \Delta\varepsilon\left(\hat{\boldsymbol{n}}_x \partial_x S_e + \hat{\boldsymbol{n}}_y \partial_y S_e\right)^2. \end{aligned}$$

We do not take into account reflections inside a LC film, which leaves only the plus sign before the radical in equation (3). Equation (3) must be solved numerically, and in the examples considered in this study, the centred finite difference method implicit in the z-direction was used; the resulting nonlinear systems of algebraic equations were solved using the nonlinear Gauss–Seidel method. After finding S_o and S_e, one can determine the directions of the electric vectors of the ordinary **o** and extraordinary **e** waves using the same eigenvalue equation. To determine the corresponding complex amplitudes E_o and E_e of these waves, higher (next) order terms in the k_0^{-1} expansion must be considered. As a result, the whole vector of the electric field can be presented as

$$\begin{aligned} \mathbf{E}^{(0)}(\mathbf{r}) = {} & E_\mathrm{o}\mathbf{o}\exp(\mathrm{i}k_0 S_\mathrm{o}) + E_\mathrm{e}\mathbf{e}\exp(\mathrm{i}k_0 S_\mathrm{e}) \\ & + (E_\mathrm{s}\mathbf{s}/\mathrm{i}k_0)\exp[\mathrm{i}k_0(S_\mathrm{o} + S_\mathrm{e})/2]. \end{aligned} \tag{4}$$

From a physical point of view, the last term in equation (4) provides the coupling between the ordinary and extraordinary waves. This term is unavoidable: if one drops it and substitutes equation (4) into (2), one would obtain three differential equations to determine only two amplitudes E_o and E_e (which is impossible in the general case). This term is important in regions (like a wall defect or near-substrate regions) where the characteristic anisotropy strength Δn (birefringence) can be of order $1/k_0 l$ (in these regions the characteristic scale of the medium inhomogeneity l is of the order of the correlation length ξ and is relatively small at high voltages). Substituting this expression into the time-harmonic wave equation (2) and combining terms with first power of k_0^{-1}, one can derive the following equations for the amplitudes E_o, E_e and E_s:

$$e_1 G^\mathrm{o}_{ik}(E_\mathrm{o} o_k) + e_2 G^e_{ik}(E_e e_k) = E_\mathrm{s} A_i \tag{5}$$

where $i = x,\ y,\ z$, $e_{1,2} = \exp(\pm \mathrm{i}k_0 \Delta S)$, and $\Delta S = S_\mathrm{e} - S_\mathrm{o}$. In these equations $A_i = \varepsilon_{ik} s_k$

$$\begin{aligned} G^\mathrm{o}_{ik}(E_\mathrm{o} o_k) = {} & 2\ \partial_k S_\mathrm{o} \partial_k (E_\mathrm{o} o_i) - \partial_i S_\mathrm{o} \partial_k (E_\mathrm{o} o_k) \\ & - \partial_k S_\mathrm{o} \partial_i (E_\mathrm{o} o_k) \\ G^\mathrm{e}_{ik}(E_e e_k) = {} & \partial_k S_e \partial_k (E_\mathrm{e} e_i) + \partial_k [\partial_k S_\mathrm{e} (E_\mathrm{e} e_i)] \\ & - \partial_i [\partial_k S_\mathrm{e} (E_\mathrm{e} e_k)] - \partial_i S_\mathrm{e} \partial_k (E_\mathrm{e} e_k) \end{aligned}$$

and ∂_k denotes differentiating with respect x_k. As one finds, equations (5) does not contain space derivatives of the amplitude E_s. This is a consequence of a specific choice of vector **s** in this study: $\mathbf{s} = \nabla(S_\mathrm{o} + S_\mathrm{e}) / |\nabla(S_\mathrm{o} + S_\mathrm{e})|$. Eliminating E_s from equations (5) gives a final set of two first order differential equations for the unknown complex amplitudes E_o and E_e of the ordinary and extraordinary waves:

$$\begin{aligned} & A_z\left[e_1\ G^\mathrm{o}_{xk}(E_\mathrm{o} o_k) + e_2 G^e_{xk}(E_\mathrm{e} e_k)\right] = A_x \\ & \left[e_1 G^\mathrm{o}_{zk}(E_\mathrm{o} o_k) + e_2\ G^e_{zk}(E_\mathrm{e} e_k)\right] \end{aligned} \tag{6}$$

and

$$\begin{aligned} & A_z\left[e_1\ G^\mathrm{o}_{yk}(E_\mathrm{o} o_k) + e_2 G^e_{yk}(E_\mathrm{e} e_k)\right] = A_y \\ & \left[e_1 G^\mathrm{o}_{zk}(E_\mathrm{o} o_k) + e_2\ G^e_{zk}(E_\mathrm{e} e_k)\right]. \end{aligned} \tag{7}$$

Examples of the numerical solution of these equations with appropriate boundary conditions will be considered in § 3. Let us discuss here an important question concerning instabilities that can arise during the solution of the amplitude equations (6) and (7). These equations may be numerically solved in two ways. First, one can develop an 'exact' solution, produced by successivly eliminating unknowns at a particular z-level; second, a solution, may be produced by the iterative Gauss–Seidel method at each mesh point (which is easier to code, especially in a 3D case). The two solutions may not coincide for the following

Downloaded At: 16:42 25 January 2011

reason. In the case when solutions are found iteratively, there is a possibility of numerical instability (or divergence) at some mesh points. The cause is that the directions of the wave vectors of the ordinary and extraordinary waves at these points almost coincide with the director, and the difference between the ordinary and extraordinary waves almost disappears. On the other hand, from a mathematical point of view, one has to solve a system of four linear inhomogeneous equations (for the real and imaginary parts of E_o and E_e) to find the complex amplitudes at a particular point. Because of the above-mentioned degeneracy between the ordinary and extraordinary waves, the 'driving force', which causes the polarizations **o** and **e** to acquire unique positions at each mesh point, is almost absent at a point of degeneracy, and the eigenvectors **o** and **e** may become almost parallel or antiparallel (at random) at some iteration step, which causes the corresponding determinant DET of the system of the four linear equations to be very small, and this can be a root of the instability. At the same time, this kind of divergence is a 'mathematical' one: it does not appear if one solves exactly (numerically) the amplitude equations, and is a consequence of the particular way of solving the problem. Thus, to produce the iterative solution, we have to find a way to remove this difficulty. The way is not unique. The simplest and, in our opinion, an effective way to remove this problem can be explained (for the case of a 3D cell) as follows. The idea is to average E_i (where i stands for the ordinary and extraordinary waves) at a 'divergent' point $\mathbf{r}_d=(x, y, z)$ between the four neighbouring mesh points instead of iterating the amplitude equations at this point:

$$E_i(x, y, z)=[E_i(x+\Delta x, y+\Delta y, z)+E_i(x+\Delta x, y-\Delta y, z) + E_i(x-\Delta x, y+\Delta y, z)+E_i(x-\Delta x, y-\Delta y, z)]/4. \quad (8)$$

To select the divergent points, we introduce a small positive parameter CUT, and a condition $|\mathrm{DET}|<\mathrm{CUT}$ can be used to pick up all points like $\mathbf{r}_d$ during the numerical solution of the system of the amplitude equations. Parameter CUT should be as small as possible provided that the solution is still convergent. In this case the number of mesh points at which the proper iterative procedure for finding E_i is substituted for the approximate formula (8) is minimal. If this number is very small compared with the total number of mesh points, one can expect that the produced solution will also be very close to the exact numerical one. In the case when the iterative solution converges, parameter CUT can be set to zero (or not introduced at all).

3. Application of the GOA

The developed GOA was applied to the calculation of light transmittance (i) through a (LC) film with two-dimensional director, which combines the concepts of in-plane switching and vertical alignment [21, 22], and (ii) through a three-dimensional LC cell associated with a homeotropic to multidomain-like transition [23] (HMD cell). Both cells possess systems of interdigitated electrodes located on one (2D film), or on both (HMD cell) substrates, and figures 1 and 2 show important features of the cells. Strong homeotropic anchoring and positive dielectric anisotropy are assumed (detailed description of the director properties of the cells are presented in [24–26]. The cells possess periodicity and systems of wall defects. In the case of the 2D cell, the central plane of one of these walls is the yz-plane at $x=0$. Because the director always lies in the fixed xz-plane, the wall defects are bend and splay walls. This choice of a LC cell for studying the optical properties was made to provide the possibility to compare the results of optical calculations with the corresponding results of the BPM where the latter is applicable. The HMD cell also possesses a system of wall defects, which lie approximately along vertical diagonal planes, such as the AC and BD planes in figure 2. For both structures we study the light transmittance for incident light at a wavelength $\lambda=550\,\mathrm{nm}$. A polarizer and analyser are placed on opposite sides of a cell to probe the polarization of the transmitted light. For simplicity, polarizers and analysers are treated as ideal, and their orientations are described in figures 1 and 2.

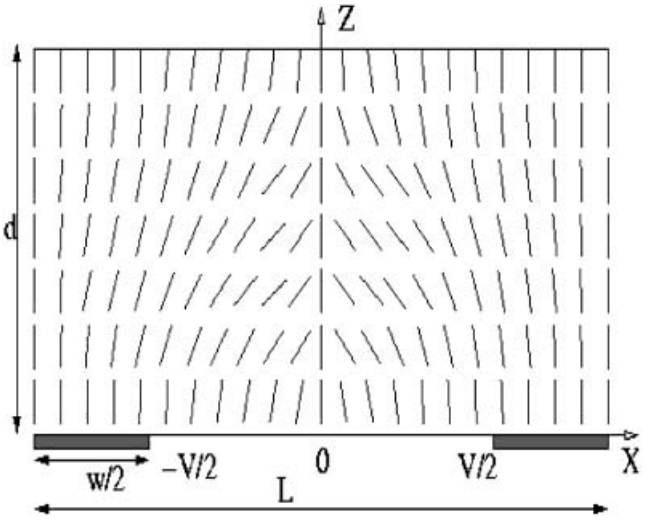

Figure 1. Schematic director profile for the 2D cell. Interval of periodicity along the x-direction is L. The transmittance axes of the polarizer and analyser make angles -45° and $+45^\circ$ with respect to the x-axis.

Downloaded At: 16:42 25 January 2011

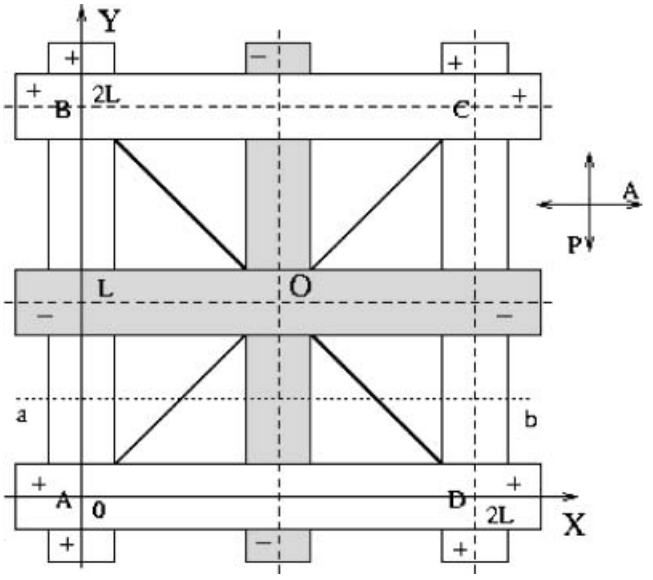

Figure 2. Top view of the HMD cell. The cell possesses $2L$ periodicity along both the x- and y-directions. The orientation of the crossed analyser and polarizer is shown in the upper right corner.

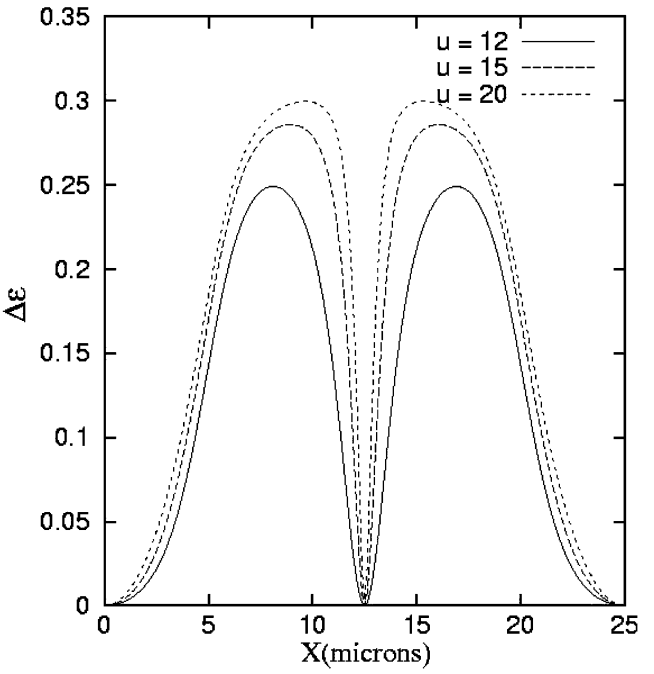

Figure 3. x-dependence of $\Delta\varepsilon = \varepsilon_{xx} - n_o^2$ for the 2D cell at different voltages.

3.1. *The 2D cell*

Experimental parameters of the 2D cell under consideration are the following. The width w of the electrode stripes, which are parallel to the y axis, is $w = 10\,\mu\text{m}$, the period $L = 25\,\mu\text{m}$, the film thickness $d = 5\,\mu\text{m}$; material parameters are: $\varepsilon_{\parallel} = 8.3$, $\varepsilon\perp = 3.1$, $K_1 = 13.2\,\text{pN}$, $K_2 = 6.55\,\text{pN}$, $K_3 = 18.4\,\text{pN}$, and the birefringence $\Delta n = 0.1$. Equation (3) for the extraordinary eikonal must be solved numerically with the following initial (at $z = 0$) and quasi-periodic conditions:

$$\partial_x S_e(z=0) = n_{gx},\ S_e(x+L,\ z) = S_e(x,\ z) + L n_{gx}$$

and the amplitude equations (6) and (7) must be solved to satisfy the periodicity conditions $E_i(x+L,\ z) = E_i(x,\ z)$.

Here $\mathbf{n}_g = \mathbf{k}_g/k_0 = (n_{gx},\ n_{gy},\ n_{gz})$, where $\mathbf{k}_g$ is the wave vector in the glass, $i = \text{o, e}$. Figure 3 illustrates the x-dependence of the value $\Delta\varepsilon = \varepsilon_{xx} - n_o^2$ drawn at $z = d/2$ (along the middle plane of the LC slab) for different voltages u. This function characterizes the deviation of the director distribution from the homeotropic one: it is equal to zero at $x = L/2$ (wall defect) and at $x = 0,\ L$. In the region between the wall defect layer and the centre of the nearest electrode, the sharpness of $\Delta\varepsilon(x)$ increases with u. We compare results of calculations of the differential light transmittance $T(x)$ produced by the GOA, BPM, and Jones method in the case of normal incidence for the same voltages as in figure 3. It is worth mentioning that for the considered 2D cell the iterative solution can be made convergent without introducing the parameter CUT mentioned above. For this purpose, one can simply choose the **k**-vector of the incidence radiation slightly off the normal with very small but non-zero k_y. Because the director is homogeneous along the y-direction, neither ∇S_o nor ∇S_e can become parallel to the director at any point inside the LC slab (the director is always in the xz-plane), and the iterative solution will converge and coincide with the exact numerical one. For this reason, only exact numerical GOA solutions are presented in figures 4–10.

For a low voltage ($u = 12\,\text{V}$ or less for this cell), all three curves essentially repeat the shape of $\Delta\varepsilon(x)$, having only the central maxima at about the same value of the x-coordinates as for the corresponding peaks of $\Delta\varepsilon(x)$ in figure 3, and the results for $T(x)$ produced by the GOA and BPM coincide and are also very close to those produced by the Jones method. When u increases, all $T(x)$ distributions flatten near their maxima, and further increase of u produces concave regions instead of peaks. One of the reasons for this is that the total birefringence along the z-axis at a particular value of the x-coordinate becomes larger than needed to reach maximum transmission, and further increase of the birefringence diminishes $T(x)$. This is illustrated in figure 4: instead of a central maximum, we have two adjacent (lateral) peaks, and this effect can be explained by any of the presented ways of optical calculation. There is, however, an additional effect that increases even more the amplitude of the lateral peaks. It is the

Downloaded At: 16:42 25 January 2011

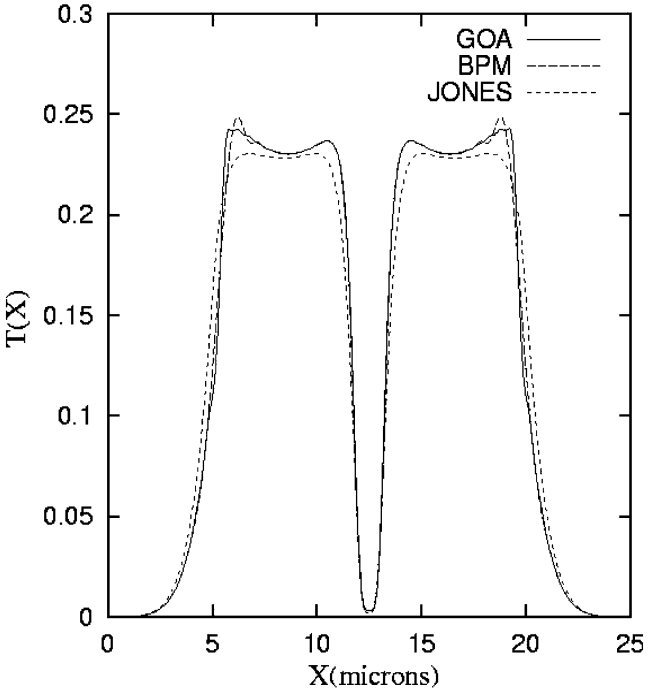

Figure 4. $T(x)$ for the experimental 2D cell at $u = 15$ V.

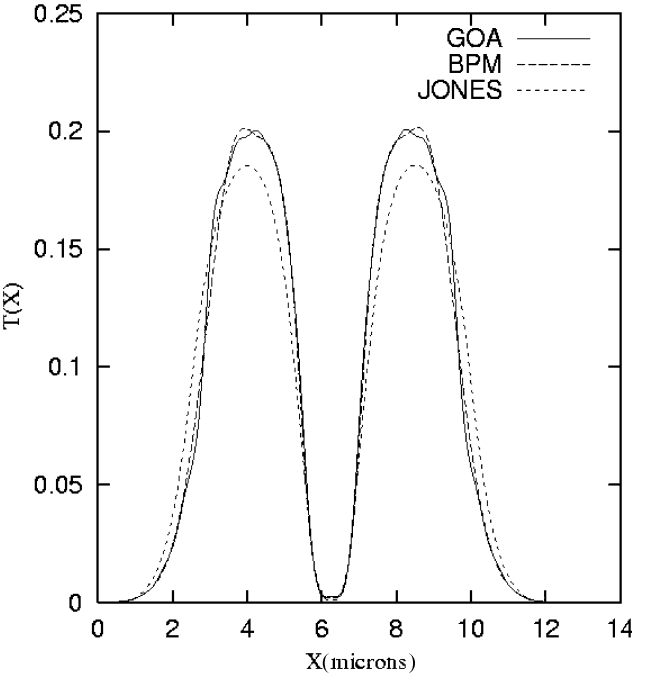

Figure 6. $T(x)$ for the reduced 2D cell ($L = 12.5$ μm) at $u = 9$ V.

Downloaded At: 16:42 25 January 2011

geometrical optics refraction due to which light rays are bent by regions with sharp changes of the index of refraction ($\Delta\varepsilon(x)$ in our case) towards the direction of larger values of $\Delta\varepsilon(x)$. As one finds from figure 4, there are two such regions at each side of the wall defect. Unlike the Jones method, the geometrical optics approach takes into account this effect, and the redistribution of the transmitted light increases the lateral maxima. As is clear from figure 4, this behaviour of $T(x)$ is in agreement with the BPM. Further increase

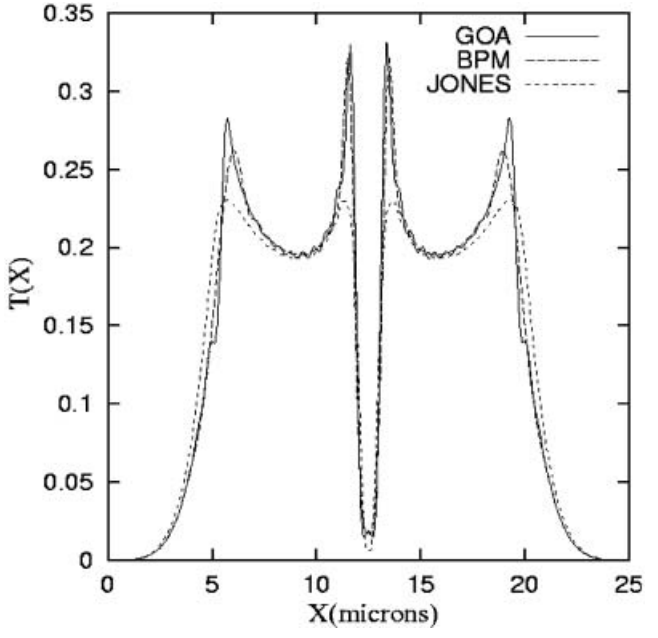

Figure 5. $T(x)$ for the experimental 2D cell at $u = 20$ V.

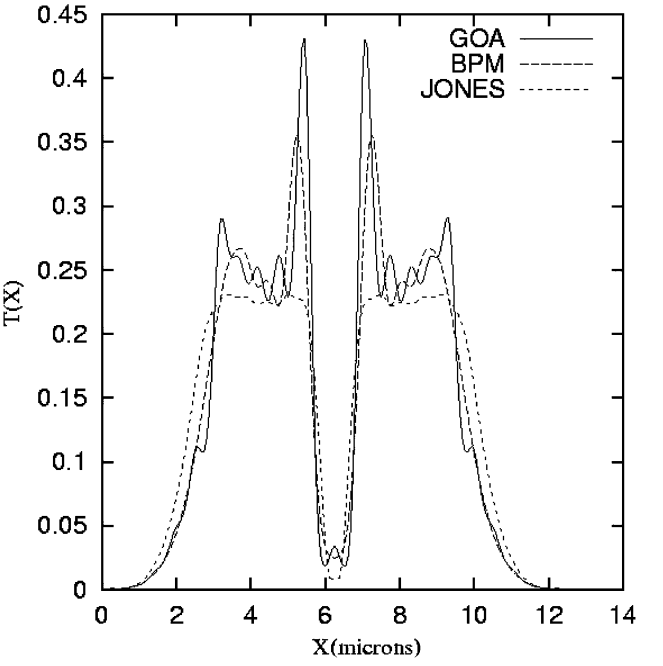

Figure 7. $T(x)$ for the reduced 2D cell ($L = 12.5$ μm) at $u = 14$ V.

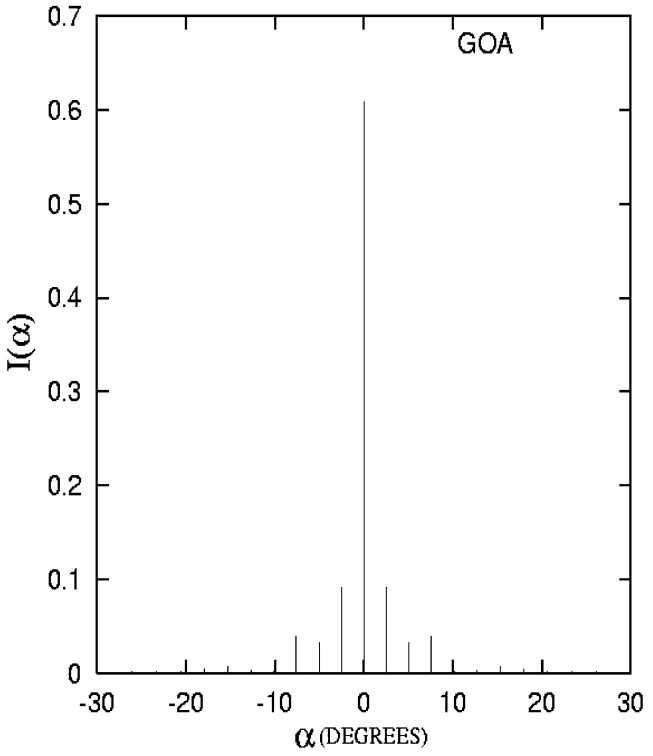

Figure 8. Diffraction spectrum for the 2D cell with $L = 12.5\,\mu m$ at $u = 14\,V$ produced from the GOA near-field result.

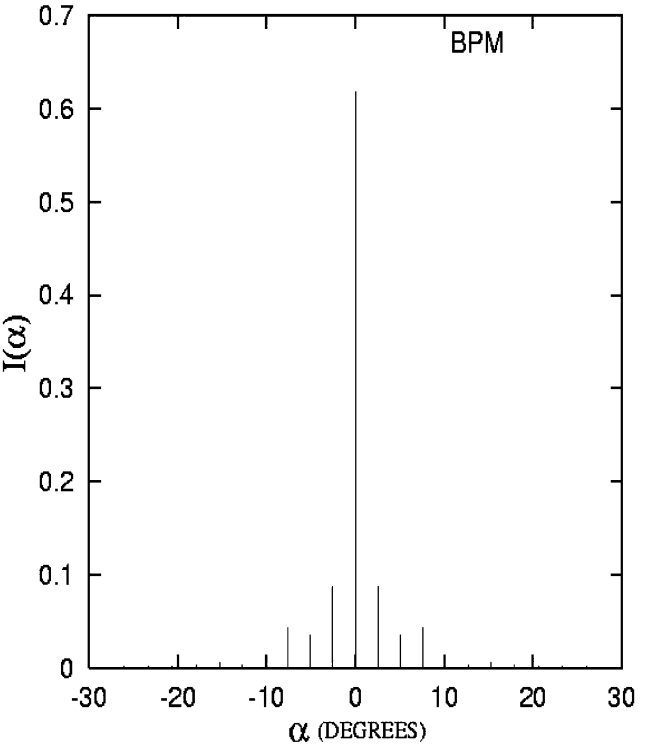

Figure 9. Diffraction spectrum for the 2D cell with $L = 12.5\,\mu m$ at $u = 14\,V$ produced from the BPM near-field result.

Downloaded At: 16:42 25 January 2011

of the voltage produces sharper maxima (figure 5). As can also be seen from figure 5, both the GOA and BPM give non-zero values $T(x)$ at the centre of the wall defect layer (unlike the Jones result), which is also due to the effect of refraction: at high u this effect is more pronounced, and a noticeable part of refracted light can even reach the centre of the wall.

It is worth mentioning that an effect of the same kind for an in-plane switching structure has been explained only by diffraction [7], which is not completely correct. The authors of [7] showed that the RGM (mentioned above) gives a peak in the differential light transmittance (unlike the Jones's zero value), which is in accordance to the experiment. However, the RGM, as well as the BPM, takes into account both the ray bending and diffraction. Because the GOA takes into consideration only the former effect and, nevertheless, reproduces properly the light transmission curve, we should accept that the effects of geometrical optics refraction are more important for the explanation of the light transmission curve behaviour. It is also clear from figure 5 that the peaks of the $T(x)$ curve produced by the BPM for high u are smoother than those from the GOA. This is because the BPM, as has already been mentioned, takes into account diffraction of light in addition to the geometrical optics features. However, as is clear from these figures, we have a very good correspondence between the GOA and BPM, which again means that the effects of light scattering and diffraction are not significant at least for the considered LC cell.

Let us now consider the same 2D LC cell but with reduced sizes in the x-direction. Figures 6 and 7 show the differential light transmittance for the case when the cell period is $L = 12.5\,\mu m$ and the electrode width is $w = 3.75\,\mu m$ (with the same cell thickness d, birefringence Δn, and material parameters as for the experimental cell). As one finds from these figures, the situation is qualitatively the same as for the cell with experimental sizes. As a result, for a low u, when the sharpness of the director distribution is less, we have a close coincidence between the GOA and BPM (figure 6). For high voltage ($u = 14\,V$ is close to the maximum of the T–V curve, or the bright state for the display with these sizes), differences between the results produced by the three methods are larger than for the bright state of the experimental cell as can be found by comparing figures 5 and 7. This is expected, because characteristic scales of the spatially varying electric

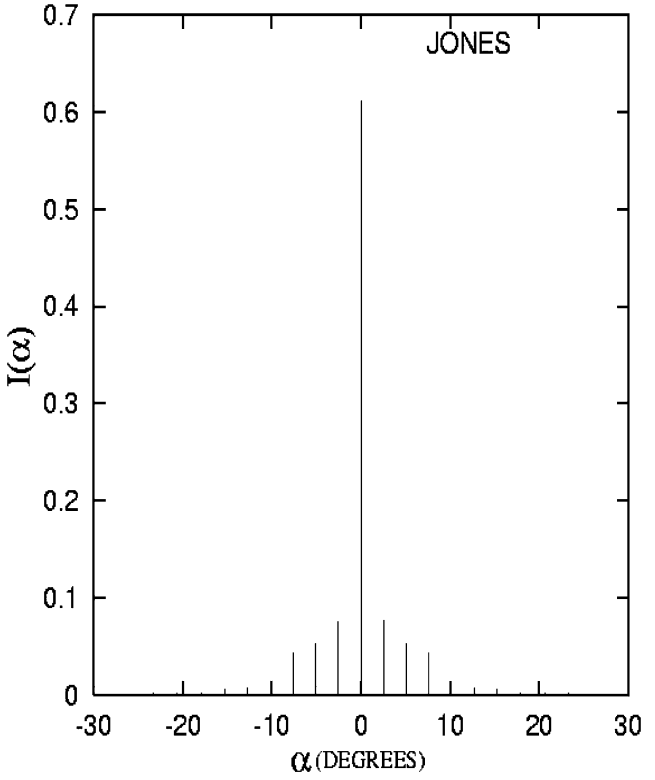

Figure 10. Diffraction spectrum for the 2D cell with $L=12.5\,\mu m$ at $u=14\,V$ produced from the Jones near-field result.

potential, and hence, the director distribution, are smaller for a cell with reduced sizes.

It is worth mentioning that the differential light transmittance $T(x)$ is very sensitive to small details of the director distribution. Moreover, it depends, in particular, on such circumstantial parameters of the LC cell as the thickness of the glass substrate d_g and the thickness of the ideal polarizer d_p (in this study an artificial situation when d_g and d_p are close to zero was assumed; in this case the influence of these parameters on $T(x)$ is negligible, and the differential light transmittance reflects only properties of the director distribution). In this regard it is important also to consider diffraction from the LC cell under consideration, and compare the diffraction patterns produced from the near-field results of the GOA, BPM, and the Jones method. As the averaged (over the cell period) light transmittance, the far field diffraction pattern reflects mainly features of the director distribution, and the diffraction pattern is also relatively easy to measure.

To calculate the diffraction, we use the vector Kirchhoff integral in its Fraunhofer limit, in which the electric field in the far zone is approximated by the following expression [27]:

$$\mathbf{E}(\mathbf{r}) = (\mathrm{i}/2\pi)\exp(\mathrm{i}k_0 r)\int \mathrm{d}\mathbf{x}\{\mathbf{k}\times[\mathbf{z}\times\mathbf{E}(\mathbf{x}')]\}\exp(-\mathrm{i}\boldsymbol{k}\boldsymbol{x}'). \quad (9)$$

Here 'x' means vector product, $\boldsymbol{k}=\boldsymbol{k}_0\mathbf{n}$, where $\mathbf{n}$ is a unit vector in the direction of observation, r is the distance between the cell centre and the observation point, and the integration is performed throughout some area (aperture) along the air-analyser interface with a size $2\rho\times 2\rho$. To calculate the diffracted far field, we have to substitute in equation (9) our near-field result $\mathbf{E}(\mathbf{x}')$ that is calculated at the previous stage (electric field immediately after exiting from the analyser–air interface). As is known, the diffraction pattern becomes manifest only at a distance r from a diffracting system much larger than the linear dimension of the system 2ρ. To reconcile the fact of boundedness of the cell with our previous assumption about periodicity of the cell, we assume also that 2ρ is much larger than L: $2\rho=NL$ with N of order 10 or larger. In this situation, it is possible to approximate $\mathbf{E}(\mathbf{x}')=\mathbf{E}(\boldsymbol{x}')$ in our 2D case as a Fourier series $\mathbf{E}(\mathbf{x}')=\sum \mathbf{f}_n\exp(\mathrm{i}k_L n x')$ for all coordinates x' not close to the cell edges, and $k_L=2\pi/L$. Substituting this expansion into (9) results in the corresponding series of diffraction peaks at particular angles $\alpha_n=\mathrm{a}\sin(n\lambda/L)$ with amplitudes $\mathbf{e}_n$ and intensities $|\mathbf{e}_n|^2=|f_{nx}|^2+[1-(n\lambda/L)^2]|f_{ny}|^2$. Figures 8, 9, and 10 show the normalized intensities $I(\alpha_n)=|e_n|^2\Big/\sum_k |e_k|^2$ of diffraction patterns produced from the near-field results of the GOA, BPM, and Jones method. As can be seen from the figures, even for a relatively high voltage the diffraction spectra produced from the GOA and BPM appear identical, and different from the one produced by the Jones method.

3.2. *The HMD cell*

Again, as in the previous 2D case, equation (3) for the extraordinary eikonal, as well as the amplitude equations (6) and (7), must be solved numerically with the following conditions:

$$\partial_x S_e(z=0)=n_{gx},\ \partial_y S_e(z=0)=n_{gy},$$
$$S_e(x+2L,y,z)=S_e(x,y,z)+2Ln_{gx},$$
$$S_e(x,y+2L,z)=S_e(x,y,z)+2Ln_{gy}$$
$$E_i(x+2L,y,z)=E_i(x,y,z),\ E_i(x,y+2L,z)=E_i(x,y,z).$$

The results of application of the GOA to the HMD cell are shown in figures 11–18 for the case of normal incidence when light is travelling from beneath the cell.

Downloaded At: 16:42 25 January 2011

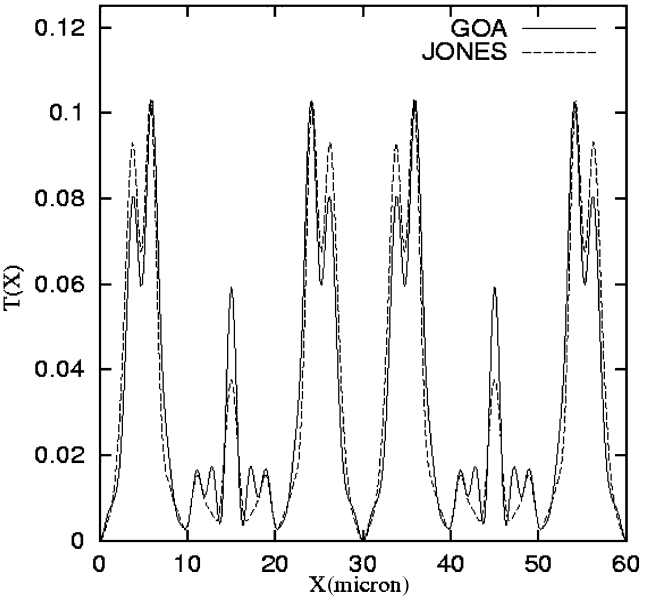

Figure 11. $T(x)$ for the HMD cell ($L=30\,\mu m$, $w=10\,\mu m$, $u=20\,V$, and $\Delta n=0.15$).

Figures 11, 12 and 17, 18 show the differential light transmittance T along the line ab (see figure 2): $T(x)\equiv T(x,\ y=L/2)$. Figures 11, 17 and 18 describe the HMD cell with geometrical sizes and birefringence as in the experiment [23]: $L=30\,\mu m$, electrode width $w=10\,\mu m$, $d=5\,\mu m$, and $\Delta n=0.088$. The rest of the figures show optical properties of the HMD cell with reduced geometrical sizes.

As was shown in the case of the 2D cell, if the iterative solution converges, it coincides with the exact numerical solution. When the iterative solution fails to converge, the difficulty can be removed as was explained in §2. It is clear, that if one chooses

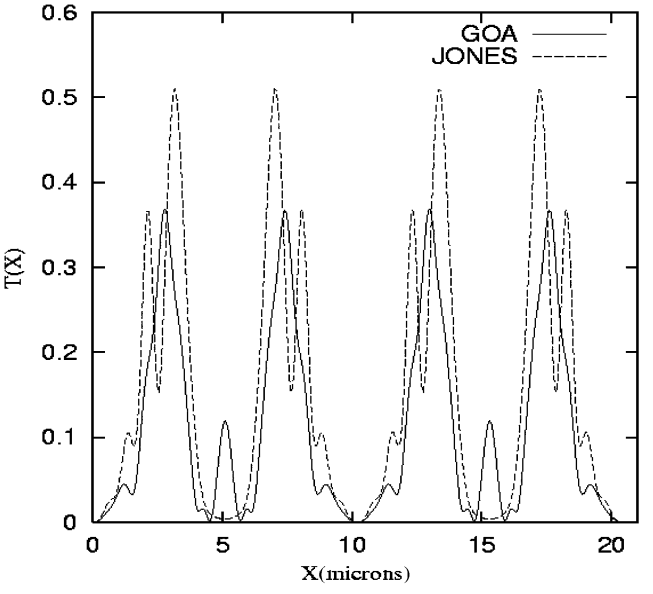

Figure 12. $T(x)$ for the HMD cell ($L=10\,\mu m$, $w=3.4\,\mu m$, $u=12\,V$, and $\Delta n=0.12$).

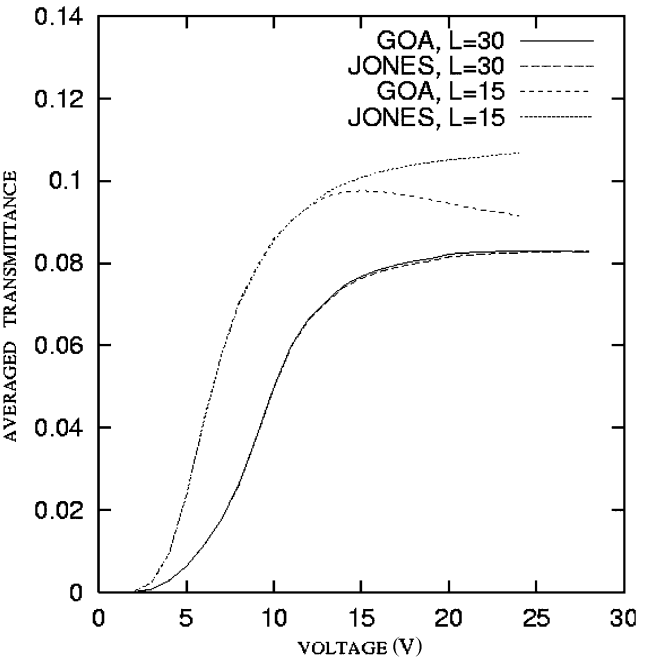

Figure 13. Averaged light transmittances for the experimental and reduced ($L=15\,\mu m$, $w=5\,\mu m$) HMD cells with $\Delta n=0.088$.

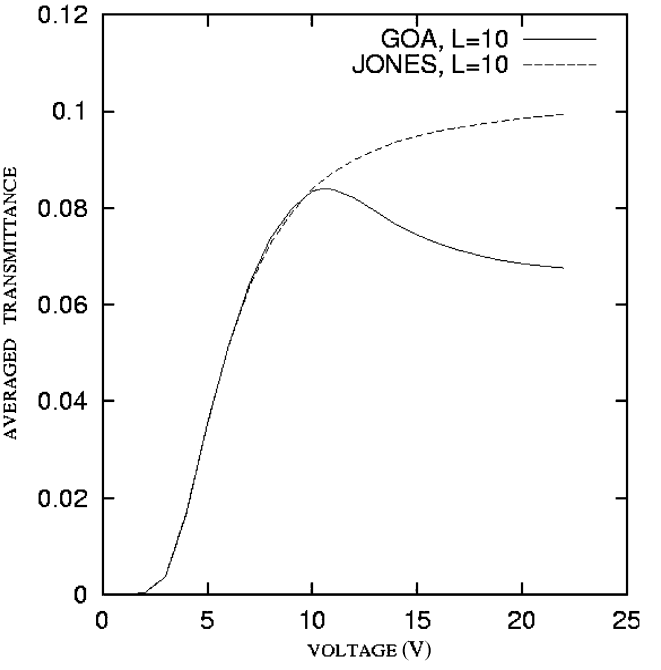

Figure 14. Averaged light transmittances for the reduced ($L=10\,\mu m$, $w=3.4\,\mu m$) HMD cell with $\Delta n=0.088$.

Downloaded At: 16:42 25 January 2011

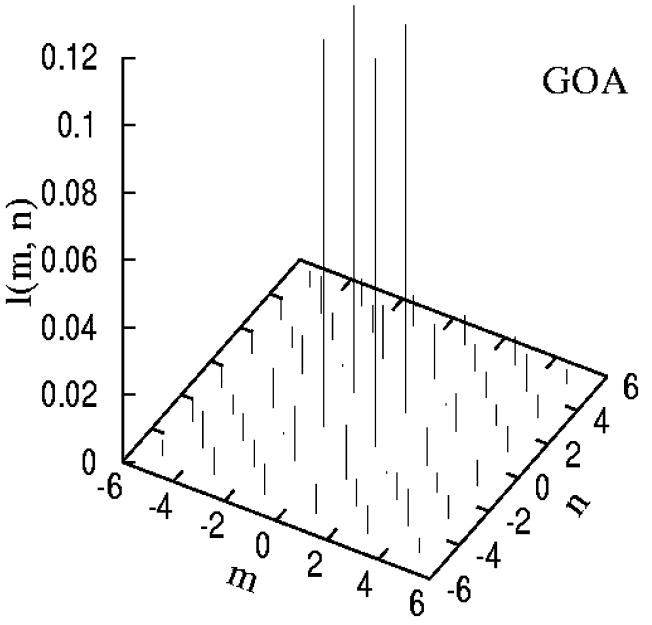

Figure 15. Diffraction spectrum for the HMD cell ($L=10\,\mu$m, $w=3.4\,\mu$m, and $\Delta n=0.12$) at $u=12$ V produced from the GOA near-field result.

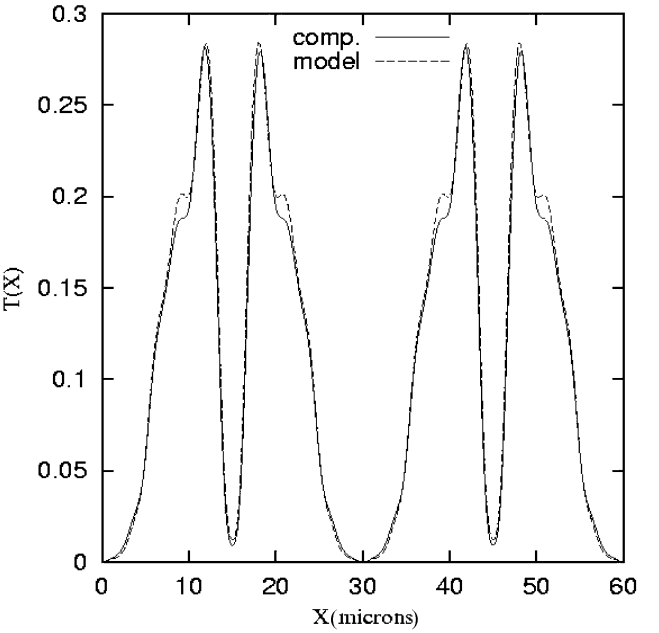

Figure 17. $T(x)$ for the model and direct computer calculations for the experimental HMD cell at $u=14$ V.

parameter CUT as small as possible to provide, nevertheless, convergence, the number of 'divergent' points may be very small compared with the whole number of usual ('convergent') mesh points at a fixed value of the z-coordinate, and one can expect that the solution will also be very close to the exact solution.

Indeed, our study showed that in all cases considered here (including the HMD cell with reduced sizes) the total number of the divergent points at each z-level, for which the solution still exists, is about 0.1% of the total number of mesh points on the z-level. Moreover, if one increases CUT an order of magnitude compared with its minimal value, then both iterative GOA solutions

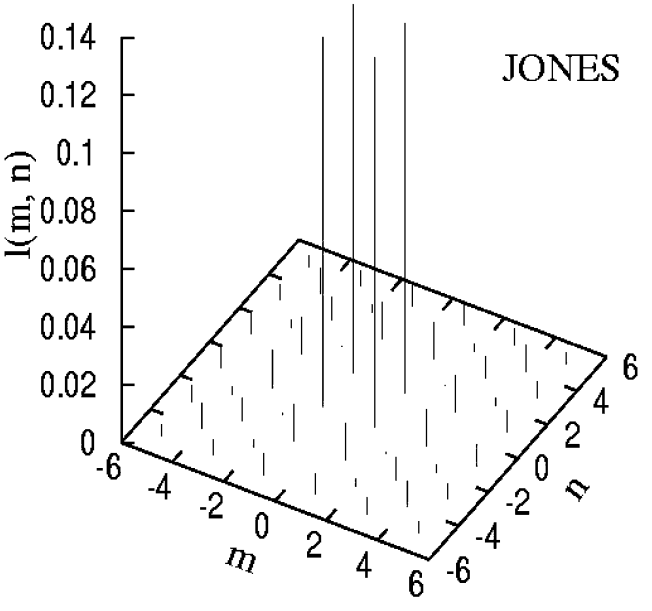

Figure 16. Diffraction spectra for the HMD cell ($L=10\,\mu$m, $w=3.4\,\mu$m, and $\Delta n=0.12$) at $u=12$ V produced from the Jones near-field results.

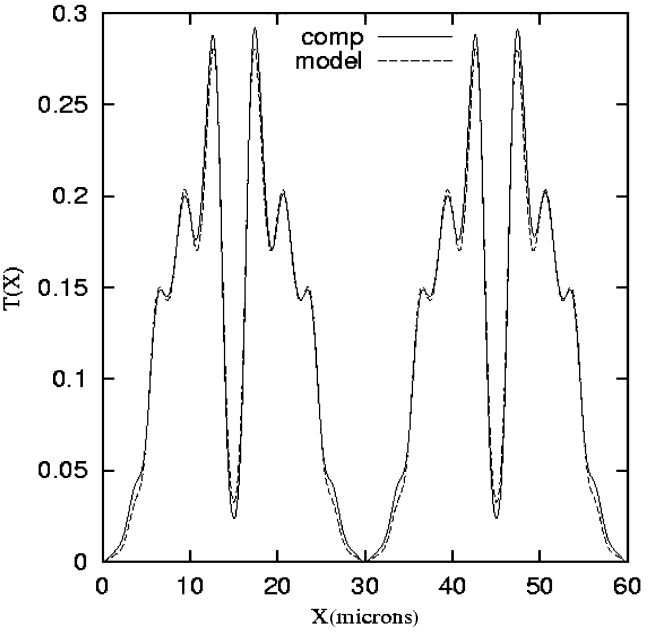

Figure 18. $T(x)$ for the model and direct computer calculations for the experimental HMD cell at $u=20$ V.

Downloaded At: 16:42 25 January 2011

for $T(x)$ are indistinguishably close to each other. The fact that the solutions produced do not depend noticeably on this parameter, also confirms that the produced iterative GOA solutions describe the optics properly.

Figure 11 shows a comparison between the iterative GOA and Jones solutions for the experimental HMD cell. As can be found from figures 5 and 11, differences between the results produced by the GOA and the Jones method are less for the HMD cell than for the 2D cell even for significantly larger birefringence ($\Delta n = 0.15$) than experimental ones for both 2D and 3D cells (as was shown in [20], the difference between the GOA and Jones method becomes larger when Δn increases). A possible explanation for this observation is as follows. In the 2D case, the surfaces where the director remains homeotropic at non-zero voltages are planes. However, the corresponding surfaces in the HMD cell are more complicated: they are close to the diagonal planes of the cell (like the planes AC and BD in figure 2) only for values of the z-coordinate close to the midpoint between the substrates, and deviate significantly from these diagonal planes in the near-substrate regions [26]. Due to this feature, the effect of ray focusing in the HMD cell is less pronounced than in the 2D cell. However, if we reduce the size of the HMD cell, results produced by the Jones method deviate more significantly from those produced by the GOA (see figure 12).

This is expected, because the Jones method ignores lateral director variations, which become increasingly important for a cell with smaller geometrical sizes in the x- and y-directions. At the same time, a characteristic scale of these variations, which are of the order of the electrode width w, is still much less than k_0^{-1}, and the GOA is still applicable in the case of absence of a strong ray focusing effect. As can be seen from figures 13 and 14, even the averaged light transmittance (T–V curves) produced by the Jones method deviates significantly from the GOA results: the maxima shown by the GOA for the cell with reduced sizes ($L = 15\,\mu\text{m}$ and $w = 5\,\mu\text{m}$, in figure 13, and $L = 10\,\mu\text{m}$ and $w = 3.4\,\mu\text{m}$, in figure 14) are absent in the Jones calculations. A qualitative explanation of this effect, as in the 2D case, is that the total (averaged) birefringence becomes larger than needed to reach maximum of the light transmittance.

As may be noticed from the results presented for both cells, the differences between different methods (in particular, between the GOA and Jones method) increase when voltage and birefringence increase, or cell sizes decrease. This is expected, because for larger u or smaller sizes, the director variations in transverse directions are sharper, and the corresponding spatial derivatives become increasingly important. It is also clear that for larger Δn the influence of these sharp changes of the director on optical properties is more tangible.

As in the 2D case, it is interesting to compare diffraction spectra produced from the GOA and Jones near field calculations for the HMD cell. Again, starting from the vector Kirchhoff integral (9) in the Fraunhofer approximation, and using double Fourier series for the corresponding near field result $\mathbf{E}(\mathbf{x}') = \sum_{m,n} \mathbf{f}(m, n)\exp[\mathrm{i}k_L(mx' + ny')]$, where $k_L = \pi/L$ for the HMD cell, one finds the corresponding series for the far field intensity peaks:

$$|\mathbf{e}(m, n)|^2 = |\mathbf{f}(m, n)|^2 - \{n_y \operatorname{Re}[f_x(m, n)] - n_x \operatorname{Re}[f_y(m, n)]\}^2 - \{n_y \operatorname{Im}[f_x(m, n)] - n_x \operatorname{Im}[f_y(m, n)]\}^2.$$

Here Re and Im stand for real and imaginary parts, $n_x = m\lambda/2L$, and $n_y = n\lambda/2L$. Figures 15 and 16 show normalized intensities $I(m, n) = |e(m, n)|^2 \Big/ \sum_{m,n} |e(m, n)|^2$ of diffraction peaks produced from the near-field results of the GOA and Jones method. Unlike the 2D case, there are four major peaks in the directions determined by vector $\mathbf{N} = (m, n)$ with $\mathbf{N} = (1, 1)$, $(1, -1)$, $(-1, 1)$, and $(-1, -1)$. This is a consequence of a particular symmetry of the HMD cell [26]. As is clear from the figure, the GOA and Jones diffraction spectra are different from each other for the case of the HMD cell with reduced size ($L = 10\,\mu\text{m}$, $w = 3.4\,\mu\text{m}$). This result is expected in view of figure 12, and is analogous to the observations illustrated in figures 8–10 for the 2D cell.

Finally, figures 17 and 18 display $T(x)$ for the director patterns calculated in two ways: using the simplified model proposed in [24–26] and direct computer calculation for two different voltages. The model can be used for studying director distributions in 2D and 3D cells and provides a fast and accurate method for the calculation of director fields for LC cells. The main idea of the model is to solve numerically the dynamic equation $\gamma_1 \partial_t \hat{\boldsymbol{n}} = -\delta F/\delta \hat{\boldsymbol{n}}$ for the director $\hat{\boldsymbol{n}}$ using a corresponding exact expression for the free energy F but an approximate analytical expression for the electric field, produced by the model. In contrast, currently used methods of direct computer solution (e.g. the relaxation method) do not use an approximate form for the electric field, but instead solve $\nabla \cdot \mathbf{D} = 0$ to get the electric field after each director update, based on the dynamic equation. As was shown, the proposed model helps us to understand better the director and electric field behaviour in liquid crystal cells and, for the HMD cell, is about 20–50 times (depending on u)

Downloaded At: 16:42 25 January 2011

faster than direct computer calculation. As can be seen, figures 17 and 18 show an excellent agreement in terms of $T(x)$ between the model and direct computer calculation, which can serve as an additional and important confirmation of the accuracy of the model. From the technological point of view, the proposed model for the director calculation (together with the GOA) constitute an accurate and fast method for LC display design, being extremely useful for finding optimal conditions for 3D and 2D LC display performance, when thousands of configurations must be analysed. In this regard it is worth mentioning that it is impossible, using additional optical elements (such as Fuji films, a- and c-plates, biaxial films), to make all gray scale levels perfect. It is usually even impossible to make both the dark and bright states perfect. Decreasing light leakage for the dark state at off-normal directions can deteriorate also quality of the viewing angle dependence of the bright state in the case of an oblique incidence. It is usually feasible, however, to find a compromise in choosing optimal conditions for the dark and bright states: to make, for example, the dark state really dark, and, at the same time, to have the bright state also reasonably good in all azimuthal directions even for large polar angles. Thus, one has to analyse first only two states (dark and bright) of a LC display. As an example, for both LC cells discussed here, the director distribution for the dark state is homeotropic and homogeneous, and one needs to find the director only for the bright state. In this situation the proposed model is especially useful and convenient: it gives the same director distribution (and the same optics) as from the direct computer solution, but is about 50 times (for the HMD cell) and about 300 times (for the 2D cell) faster. It is worth mentioning also that for the case of the bright state of the LC cells considered here, the corresponding analytical expression for the electric field used by the model is close to its high voltage asymptote, which is obviously correct, and the director model is especially well substantiated.

4. Conclusions

We have applied geometrical optics to liquid crystal films with multidimensional director variations. Important details of the GOA formalism, such as a method of removing divergences from the iterative method of solving the resulting equations for the complex amplitudes of the electromagnetic field, are described. A two-dimensional liquid crystal cell which combines the concepts of in-plane switching and vertical alignment, and a three-dimensional cell associated with a homeotropic to multidomain-like transition have been considered as examples of the GOA application. Comparisons of the results of calculations of differential and averaged light transmittance, as well as far field diffraction patterns produced by the GOA and by other methods (the BPM and Jones calculus), have been presented. The results of the analysis show that the GOA gives a more accurate description than the Jones calculus of the optics of liquid crystal films whose director variations occur on the micron scale. The geometrical optics approach is especially useful for a three-dimensional cell when the finite difference time domain method is extremely time consuming and the beam propagation method is not applicable. Being about as the fast as the Jones method, the GOA, together with the simplified director model considered previously, constitute an accurate and fast method for LC display design, which could be extremely useful when thousands of configurations must be analysed to find optimal conditions for two- and three-dimensional LC display performance.

We acknowledge support from the NASA Space Communications Project under grant number NAG3-2539. The work of E. C. G. Jr is supported by the National Foundation under Grant No. DMS-0107761.

References

[1] Berreman, D. W., 1973, *J. opt. Soc. Am.*, **63,** 1374.
[2] Lien, A., 1997, *Liq. Cryst.*, **22,** 171.
[3] Titus, C., Bos, P., and Kelly, J., 1999, *SID Symp. Dig.*, **99,** 624.
[4] Taflove, A., and Hagness, S. C., 2000, *Computational Electrodynamics: The Finite-Difference Time-Domain Method* (Artech House).
[5] Brown, V., Kriezis, E. E., and Elston, S. J., 2002, *J. appl. Phys.*, **91,** 3495.
[6] Amarasinghe, N. D., Gartland, E. C. Jr., and Kelly, J. R., 2004, *J. opt. Soc. Am.*, (in the press).
[7] Peverini, O. A., Olivero, D., Oldano, C., de Boer, D.-K. G., Orta, R., and Tascone, R., 1999, *J. opt. Soc. Am. A*, **19,** 1901.
[8] Olivero, D., and Oldano, C., 2003, *Liq. Cryst.*, **30,** 345.
[9] Kriezis, E. E., and Elston, S. J., 1999, *J. mod. Opt.*, **46,** 1201.
[10] Kriezis, E. E., and Elston, E. E., 1999, *Liq. Cryst.*, **26,** 1663.
[11] Kriezis, E. E., and Elston, S. J., 2000, *Appl. Opt.*, **39,** 5707.
[12] Fuki, A. A., Kravtsov, Y. A., and Naida, O. N., 1998, *Geometrical Optics of Weakly Anisotropic Media* (Gordon and Breach).
[13] Ong, H. L., and Meyer, R. B., 1983, *J. opt. Soc. Am.*, **73,** 167.
[14] Ong, H. L., and Meyer, R. B., 1985, *J. opt. Soc. Am. A*, **2,** 198.
[15] Kosmopoulos, J. A., and Zenginoglou, H. M., 1987, *Appl. Opt.*, **26,** 1714.
[16] Zenginoglou, H. M., and Kosmopoulos, J. A., 1989, *Appl. Opt.*, **28,** 3516.
[17] Reyes, J. A., 1998, *Phys. Rev. E*, **57,** 6700.
[18] Liu, W., Kelly, J., and Chen, J., 1999, *Jpn. J. appl. Phys.*, **38,** 2779.

Downloaded At: 16:42 25 January 2011

[19] LIU, W., and KELLY, J., 2001, *Mol. Cryst. liq. Cryst.*, **359,** 647.
[20] PANASYUK, G., KELLY, J., GARTLAND, E. C., and ALLENDER, D. W., 2003, *Phys. Rev. E*, **67,** 041702.
[21] KIM, K. H., PARK, S. B., SHIM, J. U., CHEN, J., and SOUK, J. H., 1997, in *Proceedings of the Fourth International Display Workshops*, p. 175.
[22] LEE, S. H., KIM, H. Y., JUNG, T. K., PARK, I. C., LEE, Y. H., RHO, B. G., PARK, J. S., and PARK, H. S., 1997, in *Proceedings of the Fourth International Display Workshops*, p. 9.
[23] LEE, S. H., KIM, H. Y., LEE, Y. H., PARK, I. C., RHO, B. G., GALABOVA, H. G., and ALLENDER, D. W., 1997, *J. appl. Phys. Lett.*, **73,** 470.
[24] PANASYUK, G., ALLENDER, D. W., and KELLY, J., 2001, *J. appl. Phys.*, **89,** 4784.
[25] PANASYUK, G., ALLENDER, D. W., and KELLY, J., 2001, *SID Symp. Dig.*, **32,** 850.
[26] PANASYUK, G., and ALLENDER, D. W., 2002, *J. appl. Phys.*, **91,** 9603.
[27] JACKSON, D., 1963, *Classical Electrodynamics* (New York: John Wiley).

Downloaded At: 16:42 25 January 2011